

Article

Unravelling the Influence of Binder Typology during the Additive Manufacturing of Hybrid Multi-Channel Cylinders for Catalytic Purposes

Serena Todaro ¹, Giuseppe Bonura ^{1,*}, Alessandro Cajumi ², Mariarita Santoro ¹, Fabrizio Randazzo ¹, Giosuè Giacoppo ¹, Francesco Frusteri ¹ and Catia Cannilla ^{1,*}

- ¹ Consiglio Nazionale delle Ricerche, Istituto di Tecnologie Avanzate per l'Energia "Nicola Giordano", Via S. Lucia Sopra Contesse, 5, I-98126 Messina, Italy; serena.todaro@cnr.it (S.T.); mariarita.santoro@cnr.it (M.S.); fabrizio.randazzo@cnr.it (F.R.); giosue.giacoppo@cnr.it (G.G.); francesco.frusteri@cnr.it (F.F.)
- ² Dipartimento di Ingegneria, Università di Messina, C.da Di Dio, I-98166 Messina, Italy; alessandro.cajumi@gmail.com
- * Correspondence: giuseppe.bonura@cnr.it (G.B.); catia.cannilla@cnr.it (C.C.)

Abstract: In this work, a 3D printing methodology based on the robocasting of catalytic ink pastes was applied to obtain structured matrix-like cylinders as innovative materials for an effective utilization of carbon dioxide. The influence of three different binders (i.e., PEI, HPMC and MC) on the physio-chemical, mechanical and catalytic properties of multi-channel monoliths was studied against a reference binder-free powdered system in order to envisage the effectiveness of the printing procedure in realizing hybrid advanced materials at a higher control and reproducibility than from traditional preparation techniques. In terms of textural and structural properties, the micro-extruded 3D cylinders only evidenced a slight difference in terms of relative crystallinity, with minor effects on the surface area exposure in relation to the specific binder used during the direct ink writing process. More importantly, the typology of binder significantly affected the rheological properties of the catalytic ink, with the need of a controlled viscosity to ensure a suitable thixotropic behaviour of the extrudable pastes, finally determining an optimal mechanical resistance of the final 3D monolith. The experimental validation of the hybrid multi-channel cylinders under conditions of CO₂ hydrogenation demonstrated the great potential of additive manufacturing in the realization of catalyst architectures characterized by unique features and fidelity scarcely reproducible via conventional synthetic techniques.

Keywords: additive manufacturing; direct ink writing; 3D printing; robocasting; hybrid catalysts; energy materials; CCU



Citation: Todaro, S.; Bonura, G.; Cajumi, A.; Santoro, M.; Randazzo, F.; Giacoppo, G.; Frusteri, F.; Cannilla, C. Unravelling the Influence of Binder Typology during the Additive Manufacturing of Hybrid Multi-Channel Cylinders for Catalytic Purposes. *Catalysts* **2024**, *14*, 101. <https://doi.org/10.3390/catal14020101>

Academic Editor: Miguel Angel Centeno

Received: 30 December 2023
Revised: 20 January 2024
Accepted: 23 January 2024
Published: 25 January 2024



Copyright: © 2024 by the authors. Licensee MDPI, Basel, Switzerland. This article is an open access article distributed under the terms and conditions of the Creative Commons Attribution (CC BY) license (<https://creativecommons.org/licenses/by/4.0/>).

1. Introduction

Due to the overexploitation of fossil sources, the release into the atmosphere of greenhouse gases, such as carbon dioxide, causes environmental issues and dramatically influences climate change. In addition, the progressive depletion of fossil fuel reserves makes their procurement increasingly problematic and expensive [1,2]. Therefore, creating a new energy scenario established on the green transition from traditional fossil fuels to alternative e-fuels with a net-zero carbon footprint may help determine a more sustainable and efficient energy economy in the short–medium term.

On this road to decarbonization, the technologies based on Carbon Capture and Utilization (CCU) are currently attracting particular attention, considering their potential to realize an effective way of recycling carbon dioxide via its catalytic conversion into valuable alternative fuels in the presence of renewable hydrogen [3–6].

An increasing effort is currently being delivered in the design of effective catalytic materials for the CO₂ hydrogenation into methanol or dimethyl ether, pointing out how

the development of innovative multi-functional systems can really ensure a long-range synergy among sites of a different nature, as superior to the random mixing of preformed catalysts only holding a unique functionality. Nevertheless, a consensus too limited on the key features of effective multi-site systems operating under CO₂ hydrogenation conditions still demands further optimization of the catalyst design, considering that the conventional procedures adopted for their synthesis allow neither a perfect control over site distribution or fine tuning of the physio-chemical properties or catalyst reproducibility, always requiring the experimental validation of the prepared samples followed by factitious normalization of data in an attempt to rationalize the catalytic behaviour. All of these aspects assume particular relevance if looking at the recent interest in hybrid catalysis as a viable solution for integrating equilibrium-limited cascade reactions in one single reactor, so to deliver new process chains at a higher conversion rate and productivity than conventional multi-step processes. For instance, in the case of dimethyl ether synthesis, the one-pot combination of the two catalytic steps related to primary methanol synthesis and secondary methanol dehydration can overcome the thermodynamic restrictions behind the CO₂ conversion rate [7–9], necessarily resulting in the development of hybrid formulations, integrating metal-oxide(s) and acidic sites at the local level in order to reach a high catalytic performance [10,11].

In the last few years, additive manufacturing, commonly known as 3D printing, has been proposed as the silver bullet in the field of preparation of advanced materials, due to the possibility of developing multi-faceted architectures at controlled geometry and features scalability. Unlike subtractive manufacturing, where an item is realized via computer numerical control (CNC) machining with the removal of materials from a bulk structure, additive manufacturing is a novel 3D technique that can realize complex geometries from the base upwards, by adding successive layers to create the final product [12]. Among the various types of strategies behind additive manufacturing, direct ink writing (DIW) uses a material at controlled rheological properties as an ink to be squeezed out through a syringe nozzle at a regulated flow rate [13], resulting in a flexible and powerful approach for the prototyping of advanced functional materials, composites and structures with unique shapes and applications in the field of polymers or resins [14–17], electrodes [18], ceramics [19], sensors [20] and reactive inks [21], usable in all technological fields of science, included biomedical applications [22,23]. In the field of catalysis, the extrusion-based method is widely utilized for obtaining a catalyst with tailored structures, with a specified shape and a suitable size for minimizing pressure drops, preserving uniform flow distribution and improving mass and heat transfer phenomena [24–26]. Among all the different additive manufacturing techniques, the direct ink writing (DIW) method takes advantage due to a higher simplicity and lower cost, also allowing promoters or active components to be directly added to the appropriate printing paste or ink [27–29].

The main purpose of this study is to define an adequate methodology of additive manufacturing of hybrid multi-channel cylinders for catalytic purposes, considering the lack of detailed information on the specificity of binder typology on the physio-chemical, mechanical and catalytic properties of 3D catalysts prepared via robocasting. Indeed, the addition of a specific binder in the ink recipe can modify the rheology of the ink, with direct effects on the textural, structural or surface properties of a 3D catalyst. As a result, the rheological properties of a printing ink, as adjustable through the use and/or loading of a specific binder, definitely play a crucial role in the performance of 3D structures for catalytic purposes.

As a powdered base for the preparation of the ink material, a previously optimized catalytic formulation for the one-pot hydrogenation of CO₂ into dimethyl ether was selected, to be combined with three different binders (i.e., PEI, HPMC and MC), well known as hydrogels and characterized by viscoelastic properties suitable for robocasting where a good shape retention capacity is a fundamental feature [30–32].

Indeed, apart from the parameters related to shape and scale of the printed material as well as the diameter of the syringe nozzle, precise manufacturing requires the right

typology of binder controlling the slurry density of the ink paste, with clear effects both on the rheology of the paste and on the mechanical properties of the final material.

2. Results and Discussion

Design and Synthesis of Hybrid Monoliths

After the micro-extrusion process was performed, the monolith shrinkage was investigated through digital microscopy to evaluate diameter, height, and row size. These measurements were conducted for the monoliths as printed, after drying and after calcination (see Table 1). First of all, it is observable that the robocasting of the catalytic ink pastes allows a perfect control on the final size of the monolith, considering that all multi-channel structures exhibit perfectly identical dimensions immediately after printing, according to the design.

Table 1. Shrinkage of monoliths as printed, after drying and calcination: (a) top view; (b) side view.

Sample	Status	Diameter (mm)	Height (mm)	Row (mm)	(a)	(b)
HYB-PEI	As printed	17.00	32.00	1.12		
HYB-PEI	Dried	15.83	28.63	1.06		
HYB-PEI	Calcined	15.63	28.33	1.01		
HYB-HPMC	As printed	17.00	32.00	1.12		
HYB-HPMC	Dried	15.82	28.03	1.01		
HYB-HPMC	Calcined	15.47	27.49	0.98		
HYB-MC	As printed	17.00	32.00	1.12		
HYB-MC	Dried	15.69	27.27	1.05		
HYB-MC	Calcined	15.35	27.05	1.01		

All samples exhibited a total mass loss of about 34–36%, with the main loss occurring at 320 °C, due to the removal of oxalate species. At 360 °C, the removal of the organic binder occurred, suggesting a temperature of 350 °C as sufficient for a complete calcination. As expected, after air drying, a decrease in size along the three dimensions caused by water evaporation was observed for all samples. After calcination, the further shrinkage was caused by the removal of CO_x species of the oxalate coprecipitated phase. This was also confirmed by the TG/DSC study performed over the dried monoliths in air flow to determine the suitable calcination temperature for achieving complete decomposition of both the precursors and of the organic binder. The temperature was raised from room temperature to 1000 °C at a heating rate of 10 °C/min, and the mass loss was recorded as a function of temperature (see Figure 1).

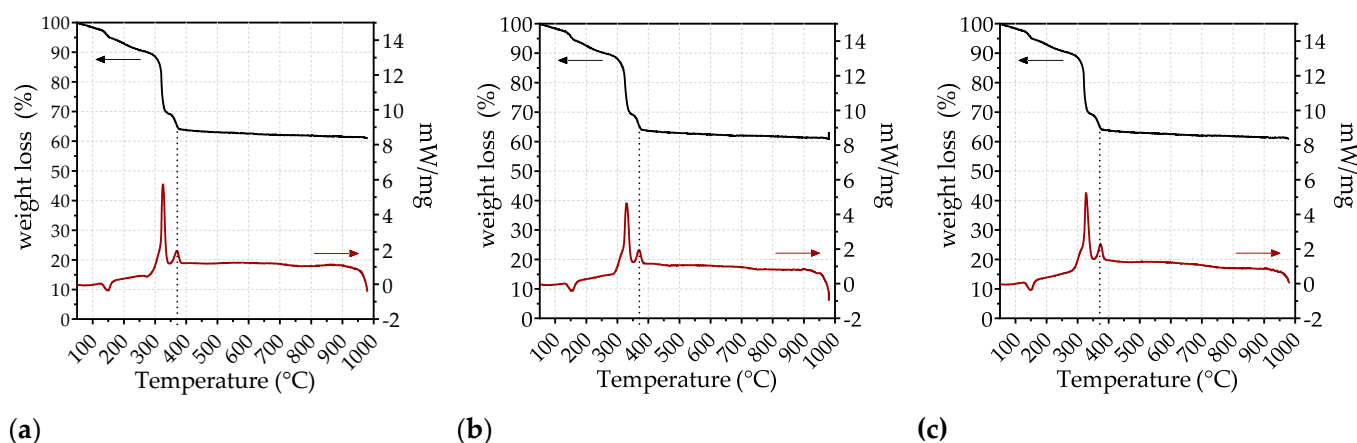


Figure 1. TG/DSC curves of the dried binder-containing powders: (a) HYB-PEI; (b) HYB-HPMC; (c) HYB-MC.

Regarding the textural properties, Table 2 reports a comparison of the main surface area (SA_{Lang}) and pore volume (PV) determined for the 3D monoliths and the bare hybrid sample (HYB). It can be stated that the printing technology certainly allows a good control of the catalyst properties, considering that the micro-extrusion procedure only determined a slight decrease in the surface area exposure ($\approx 5\%$) with respect to the powdered hybrid sample (HYB), with the pore volume remaining almost unchanged in all samples, irrespective of the binder used. In any case, it is to be underlined that XRF analysis (not shown for sake of confidentiality) revealed the presence of other elements in the printed samples (around 2 wt.%) ascribable to impurities of the inorganic co-binder, which is nevertheless necessary for the consistency of the final monolith.

Table 2. Textural properties of the investigated hybrid sample (HYB) after extrusion with the different binders.

Sample	$SA_{Lang}^{(a)}$ ($m^2 g^{-1}$)	$PV^{(a)}$ ($cm^3 g^{-1}$)
HYB-PEI	217 ± 3.4	0.21
HYB-HPMC	219 ± 2.8	0.21
HYB-MC	220 ± 3.1	0.22
HYB	235 ± 3.0	0.24

^(a) From N_2 ads/des isotherms at $-196^\circ C$.

In Figure 2, the XRD patterns of the parent hybrid catalyst HYB and the multi-channel hybrid cylinders upon calcination treatment are shown.

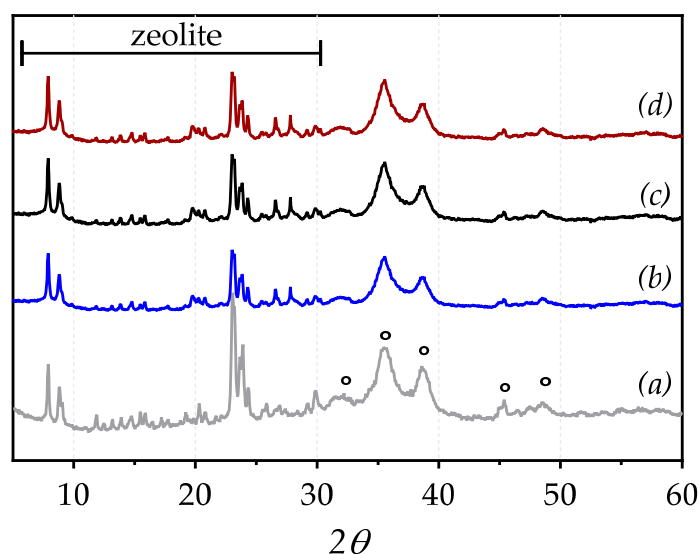


Figure 2. XRD patterns upon calcination of: (a) parent HYB catalyst; (b) HYB-PEI; (c) HYB-HPMC; (d) HYB-MC. The circles indicate the peaks selected for the determination of crystallinity.

As observed, not only the reflections of the zeolite structure (JCPDS 38–0246), but also the main oxide phases of the parent hybrid system were fully retained after the printing procedure. Instead, in terms of crystallinity, with respect to the basic reference structure, the printed samples displayed a partial loss of crystallinity, mainly associated with the typology of binder used for manufacturing of the 3D cylinders and then removed via calcination, which evidently caused more or less disordered crystalline forms, according to the following trend:

$$HYB (100\%) > HYB-MC (95\%) > HYB-HPMC (89\%) > HYB-PEI (84\%)$$

Considering that not only the composition, but also the wettability or flow behaviour represent crucial factors in the formulation and managing of ink solutions, the rheological properties of the ink must be thoroughly tailored to control the shape and span gaps of the final 3D multi-channel cylinders. If not properly prepared, the ink paste during extrusion can suffer from shear localization induced through a sudden contraction at the syringe nozzle and depend both on the extent of pressure drop at the nozzle and on the time of extrusion.

On this account, the shear stress (τ) as a function of the strain rate (γ) was determined and is shown in Figure 3.

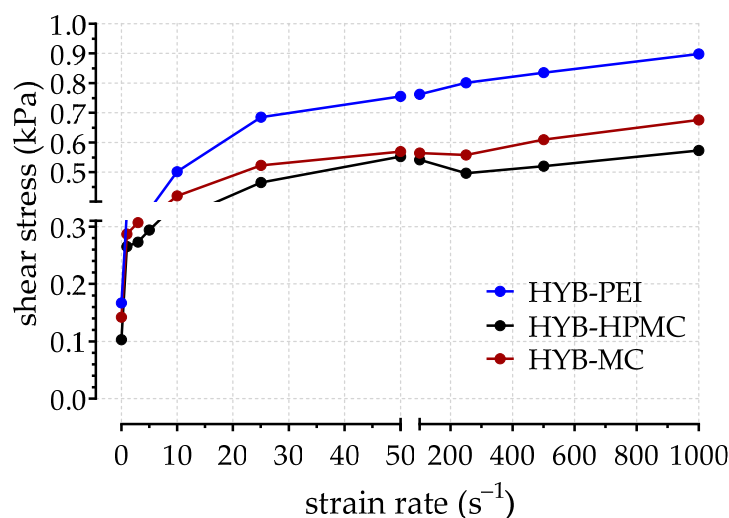


Figure 3. Shear stress–strain rate curves for the prepared catalytic ink pastes: HYB-PEI, HYB-HPMC and HYB-MC.

For all samples, the lack of a direct proportionality between the shear stress and the strain rate mirrors a pseudo-plasticity that is typical of non-Newtonian fluids, as associated to a shear thinning behaviour wherein the “apparent” viscosity is strictly dependent on the flow velocity.

In particular, the HYB-PEI sample displayed the highest yield stress, resulting about 20 and 40 Pa higher than HYB-MC and HYB-HPMC, respectively. This observed behaviour for the used ink pastes, which is typical for pseudo-plastics (or shear-thinning fluids), was also analysed using the Bingham equation (Equation (1)) over the linear high-shear region of τ versus γ curves:

$$\tau = \tau_0 + \eta_{pl} \cdot \gamma \quad (1)$$

where η_{pl} is the apparent plastic viscosity (kPa·s), and τ_0 is the Bingham yield stress (Pa), which represents the point beyond which the flow rate steadily increases with the shear stress.

As shown in Figure 4, the apparent viscosity decreased rapidly for all samples while increasing the shear rate until about 5 s^{-1} , then slowly decreasing the shear rate until the maximum shear rate of 100 s^{-1} . As a rule, high viscosity at low shear forces, then decreasing with an increase in shear rate is a characteristic feature for ink pastes undergoing pressure-regulated flows, allowing the material to flow through the nozzle until the layer-by-layer geometry is completed.

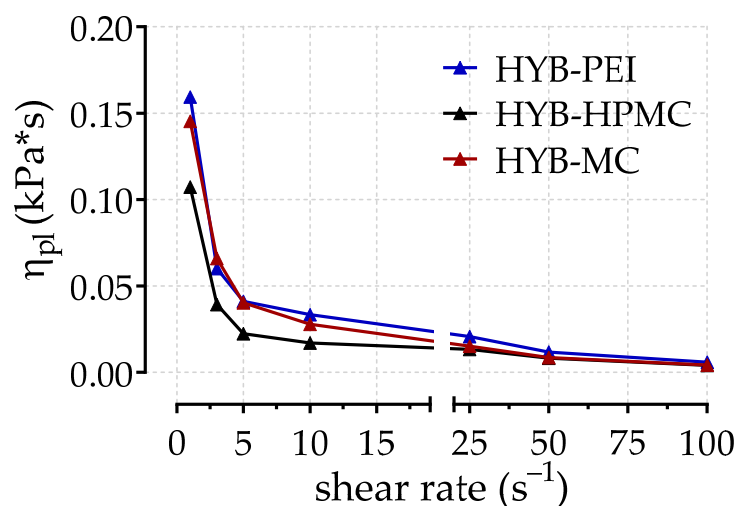


Figure 4. Apparent viscosity of the catalytic pastes as a function of shear rate at 18 °C.

To determine the mechanical resistance of the monoliths as induced by the three binders initially utilized, some compression tests were carried out on the calcined 3D multi-channel monoliths in order to evaluate possible issues preventing application in catalytic processes typically operated at both high temperature and pressure. In Figure 5, the obtained stress–strain curves are presented.

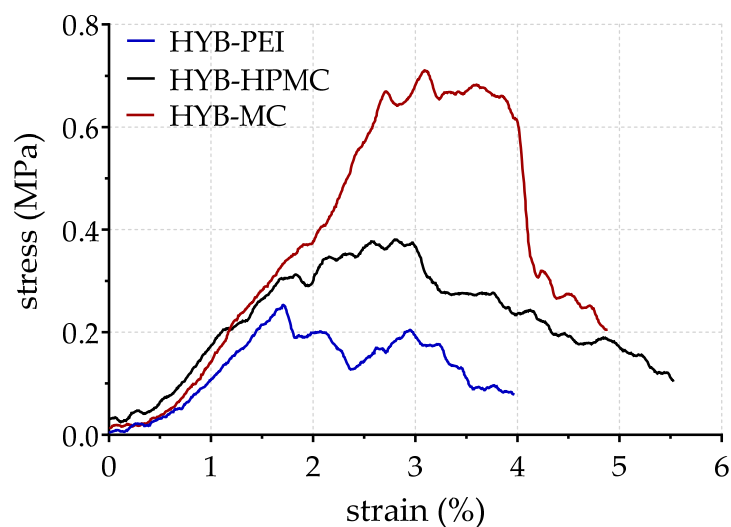


Figure 5. Compressive stress–strain curves for HYB-PEI, HYB-HPMC and HYB-MC monoliths.

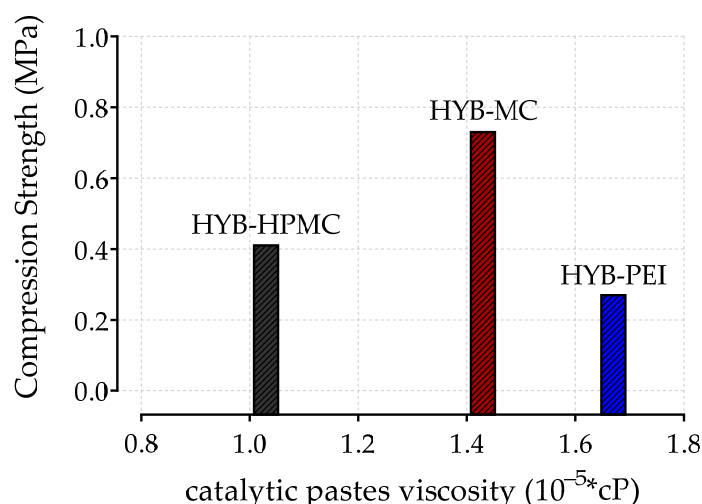
As observed, the HYB-MC sample exhibited a significantly higher mechanical resistance in respect of the other samples. This is ascribable to an intrinsic chemical structure of the methyl cellulose, allowing suitable interface bonding to limit cracks and enhance mechanical integrity upon the calcination treatment. Instead, in the case of HPMC, and more markedly of PEI, the cross-linkable networks at too-high hydrophilicity play a negative effect on the microstructure of the solid after the thermal treatment, therefore depressing the “ultimate stress” with a decrease of about 40% (≈ 0.4 MPa) and 70% (≈ 0.2 MPa), respectively, with respect to the value recorded on HYB-MC (≈ 0.7 MPa). Moreover, the slope of the stress–strain curves in the elastic region (below 1.5% of strain) was used to derive the compression modulus (M_c). The obtained values in Table 3 confirm the great influence of the binder on the monolith stiffness.

Table 3. Mechanical properties of 3D hybrid monoliths prepared with different binders.

Sample	Mc (MPa)	σ_{\max} (MPa)
HYB-PEI	0.125 ± 0.002	0.27
HYB-HPMC	0.169 ± 0.002	0.41
HYB-MC	0.201 ± 0.001	0.73

While the HYB-PEI sample exhibited a compression modulus as low as 0.125 MPa, the HYB-MC sample was characterized by the highest value (0.201 MPa), also mirroring the highest value of compression strength (σ_{\max} , 0.73 MPa).

To understand how the viscosity of the paste influenced the mechanical resistance, the σ_{\max} was then plotted as a function of the viscosity of the starting catalytic paste. It can be seen from Figure 6 that an intermediate paste viscosity leads to a greater mechanical resistance; in contrast, too high or too low viscosity values decrease the mechanical resistance of the final monolith.

**Figure 6.** Compression strength of the final monoliths as a function of the paste viscosity.

Regarding the catalytic behaviour, in Figure 7, the comparison of the performance between the powdered hybrid sample (HYB) and the HYB-MC sample, as representative for the 3D-printed cylinders, is reported in terms of CO_2 conversion (X_{CO_2} , %) and selectivity (S_x , %) to dimethyl ether (DME), methanol (MeOH) and carbon monoxide (CO), obtained at 3.0 MPa, 220 °C and a space velocity of 1000 NL/kg_{cat}/h.

Under the adopted conditions, for both samples, the CO_2 conversion attained similar values close to 10–11%, with the slightly lower value on the multi-channel HYB-MC sample being contained within the experimental error and, in any case, resulting almost identically if normalized in terms of the active phase, net of the binder concentration. In terms of selectivity, considering the absence of hydrocarbons in the reaction stream, on both catalysts, the DME represented the main product with comparable values at around 52–53%. Instead, the main differences were observed on the relative distribution of MeOH-CO, since on the 3D-printed cylinder, the MeOH selectivity resulted to be significantly higher (18.8%) than the amount formed on the powdered system (12.5%), accordingly determining a specular effect on CO selectivity, which reached a maximum value of 36.3% on the reference HYB sample and a lower value of 29.6% on the 3D sample.

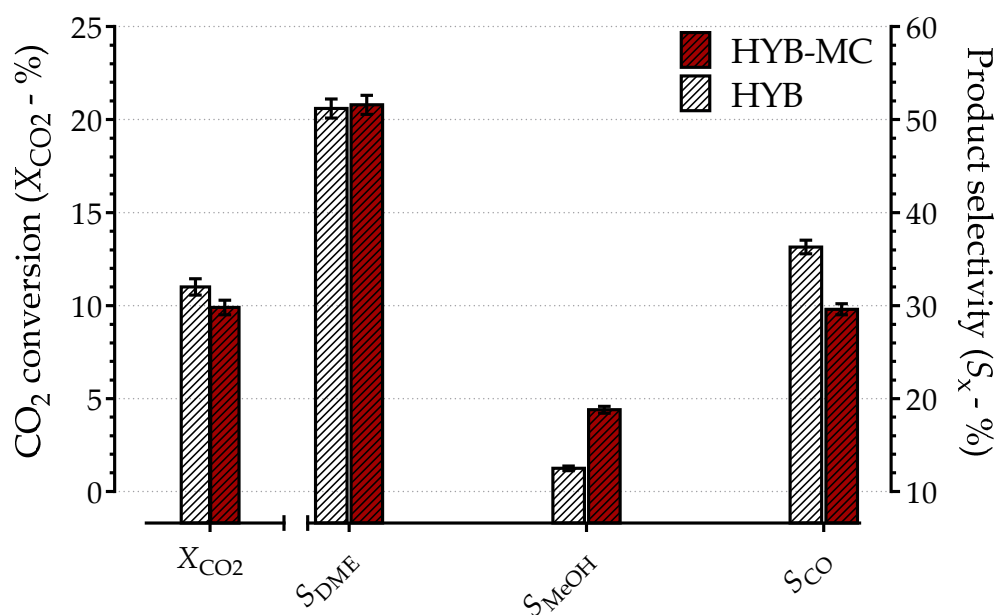


Figure 7. Activity–selectivity data during the one-pot hydrogenation of CO₂ to DME (P_R , 3.0 MPa; T_R , 220 °C; CO₂/H₂/N₂, 3/9/1 v/v; GHSV: 1000 NL/Kg_{cat}/h).

It is argued that, under similar physio-chemical properties of the investigated samples as well as similar fluid–dynamic conditions applied during the experimental runs, the observed differences recorded in the selectivity to methanol and carbon monoxide are mainly ascribable to the catalyst architecture, which in the specific case of the 3D multi-channel cylinders are also less susceptible to water deactivation, being characterized by a drainage behaviour that favours an extension of catalyst lifetime; thus, retarding the oxidation of the metallic phase that is claimed as responsible for the reforming/decomposition paths of methanol into CO [7]. Without considering additional effects (if any beneficial), on the whole, these data demonstrate the effectiveness of 3D-printed systems, with a large potential for applications in catalytic processes where only a fine optimization achievable through means of unconventional techniques (like additive manufacturing) can make their features superior than conventionally used powdered systems.

3. Materials and Methods

3.1. Catalyst Powders Synthesis and 3D Monoliths Design

Three-dimensional structures with a cylindrical shape were manufactured, starting with a hybrid metal-oxide/zeolite dry powder (herewith generally indicated as HYB), prepared by gel-oxalate coprecipitation as elsewhere described [8]. This dry powder, mechanically mixed with a suitable amount (<5 wt.%) of bentonite (Thermo Scientific, Waltham, MA, USA) as an additive for proper consistency of the slurry paste, was used as the basis for the catalytic ink undergoing micro-extrusion. Three catalytic ink pastes were prepared by mixing the catalytic powders with three different organic binders: (1) polyethyleneimine (PEI, Merck; 18,000–40,000 cP); (2) hydroxy-propyl-methyl cellulose (HPMC, Merck; viscosity 2600–5600 cP); (3) methyl cellulose (MC, Thermo Scientific, Waltham, MA, USA; viscosity 4000 cP). Then, each paste was diluted by 50 wt.% with distilled water, finally constituting with bentonite up to 14 wt.% of the final 3D hybrid composition.

All pastes were grinded through a planetary ball mill (Powteq BM40, Beijing, China) within zirconium oxide jars for 1h at 250 rpm until a good homogeneity of particles size was obtained to be extruded through the nozzle (diameter 1.1 mm). The extrusion was carried out using a customized robocasting machine (E.O.I. Tecne, Milan, Italy) equipped with a software-controlled mechanical arm where a Preeflow Eco-Pen450 syringe (Viscotec, Töging Am In, Germany) was installed, moving on an x,y,z (300 × 300 × 300 mm) stage and

connected to a precision dispenser (Techcon TS250/255, Cypress, CA, USA) to control the paste flow rate (a pressure of 4 bar at a print velocity of 12 mm s⁻¹). Based on preliminary trials, a cylindrical geometry (17 mm diameter and 32 mm height) was adopted for the manufacturing of the 3D systems, constituted using 90° alternating layers upon layers, at a row spacing of 2 mm and a row diameter of 1.1 mm, with a precise control of the interface between the extruded lines and without any issue related to possible overflow. The pastes were printed in air with a relative humidity of 60% and a temperature of 23 °C. Finally, the obtained 3D-printed monoliths were air-dried at room temperature for 24 h and then calcined at 550 °C for 2 h (1 °C/min) to remove the organic binder.

3.2. Characterization

In order to individuate the adequate calcination temperature of the catalytic pastes, a thermogravimetric analysis coupled to differential scanning calorimetry (TG-DSC) was performed using a Netzsch STA 409 thermo-balance (Selb, Germany), operating at a heating rate of 10 °C min⁻¹ from 40 to 1000 °C in static air.

The elemental composition of the samples was determined using X-ray fluorescence analysis, using a Bruker S8 TIGER spectrometer (Rheinstetten, Germany), equipped with a rhodium anode tube (power 4 kW and 75 µm Be window and LiF 220 crystal analyser). The samples were analysed as loose powders, considering the emission transitions of the main components of the catalyst.

The diffraction patterns of the prepared samples were analysed, upon crushing and sieving in the 40–70 mesh fraction, using a Bruker D8 Advance diffractometer (Rheinstetten, Germany), operating with a Ni β-filtered Cu-Kα radiation ($\lambda = 1.5406 \text{ \AA}$) in the 2θ range 5–80° at 40 kV and 40 mA and a scan step of 0.03° s⁻¹. The crystallinity was calculated by considering the area of the crystalline peaks for a specific sample in relation to the reference hybrid sample.

The surface morphology and the shrinkage of the printed monoliths after drying and calcination were measured using a fully automated digital VHX-7000 optical microscope (Keyence, Milan, Italy), provided with calibrated 2D scales and high-quality 3D models at accurate point heights and profiles. The detection of possible artefacts on the structure of the investigated architectures was made using 4K CMOS high-resolution lenses (Keyence, Milano, Italy) and high-performance lighting, which enabled minute surface details to be observed and analysed, in a magnification range of 20x to 6000x using a motorized turret.

The textural properties of the samples were determined using physical adsorption measurements of nitrogen to its boiling point (−196 °C), using a Micromeritics ASAP 2020 gas-adsorption device (Norcross, GA, USA). All calcined materials were previously crushed and sieved, with the fraction ranging from 40 to 70 mesh and collected for the measurements. The samples were first evacuated at 180 °C for 3 h, while the isotherms for the assessment of surface area (SA) were elaborated according to the Langmuir method and the micropore volume was determined using the *t*-plot approach.

The rheological properties of the catalytic pastes were carried out at 18 °C using a home-made rotational rheometer operated in a laminar flow, according the shear rate- and the shear stress-controlled protocols. Prior to the measurements, the binder-containing hybrid ink pastes were pre-sheared at 50 s⁻¹ for 1 min to obtain a homogeneous paste, followed by a resting time of 5 min, and finally sheared at a low shear rate of 0.1 s⁻¹ for 1 min until reaching the onset value of the curve, representing the static yield stress. Then, the paste was measured under a varying shear rate for 10 min, by changing the rate from 0 to 1000 s⁻¹. The plastic viscosity was determined via the intersection and slope of the shear rate curves with the shear stress. All rheological tests were carried out at a constant temperature of 18 °C, maintained constant using a water bath.

The compressive strength of the monoliths was determined using a servo-hydraulic testing machine (Italsigma, Forlì, Italy) equipped with a 12.5 kN load cell. The compression plates were mounted on the machine. The tests were performed in displacement control with an actuator speed of 1 mm/min. The trend of the force and the position of the

crosshead during the test were recorded. The highest compressive force value recorded during the test was assumed as the maximum force value. After this value, yielding occurs in the component, which leads to a reduction in the compressive force. These tests were performed over 10 specimens for each sample in order to produce statistical reliable data.

3.3. Catalytic Testing

The catalytic behaviour of the differently shaped samples was evaluated under a similar residence time and using two different fixed-bed reactors, located within rounded bars to operate in isothermal conditions and characterized by a same length of 400 mm but an internal diameter of 6.4 (for the powdered samples) or 12.8 mm (for the 3D cylindrical samples,) respectively. Prior to the measurements, the investigated samples were pre-reduced in situ at 300 °C under “pure” hydrogen, flowing at atmospheric pressure for 1 h. The catalytic measurements were performed under CO₂ hydrogenation conditions by feeding over the catalytic bed a reaction mixture CO₂/H₂/N₂ at a molar ratio of 3/9/1, at 30 bar, 220 °C and a space velocity of 1000 NL/kg_{cat}/h, also preventing possible mass or heat control by diffusion resistances. The reaction stream was analysed with a double-column GC 8000 system (Fisons, Ipswich, UK) connected to a flame ionized detector (EL980, Fisons, Ipswich, UK) and a hot wire detector (Fisons, Ipswich, UK), respectively. For the calculation of conversion–selectivity data, both internal standard and mass-balance methods were adopted, with an accuracy of ± 3% and a carbon balance close to 100% [8].

4. Conclusions

The influence of three different organic binders (i.e., PEI, HPMC and MC) on the physio-chemical, mechanical and catalytic properties of 3D multi-channel hybrid monoliths as catalytic samples for CCU applications was investigated against the basic properties of a binder-free reference powdered hybrid sample. Entering into the composition of the final monolith, a minimum addition of bentonite (<5wt.%) was also necessary to ensure the proper consistency of the slurry during printing, and was also fundamental for preventing surface cracking upon drying.

On the whole, the typology of the binder was seen to influence not only the rheological properties of the catalytic inks (like yield stress and plastic viscosity) but especially the mechanical resistance of the final 3D structures. A superior behaviour was recorded in the case of the methyl cellulose (MC), displaying the need for a paste viscosity comprised between 1.20×10^5 and 1.50×10^5 cP to ensure a compression strength as high as 0.73 MPa.

Overall, this study demonstrates the successful preparation of advanced materials for catalytic purposes using additive manufacturing, considering that the use of a specific binder entering into the catalyst composition significantly controls the mechanical properties of the final material, while retaining its key physio-chemical properties and without depressing its activity–selectivity pattern in respect of conventional reference powdered systems.

As a final message, these results can be extended to many other areas of research and development of 3D hybrid materials, so to pave the way for scaling up and industrial use against reference powdered materials.

Author Contributions: Conceptualization, G.G. and C.C.; data curation, S.T. and M.S.; funding acquisition, G.B. and F.F.; investigation, S.T. and F.R.; methodology, A.C. and G.G.; project administration, G.B.; resources, G.B. and C.C.; software, F.R.; supervision, F.F.; validation, S.T. and A.C.; writing—original draft, S.T. and A.C.; writing—review & editing, G.B. All authors have read and agreed to the published version of the manuscript.

Funding: This research was funded under the National Recovery and Resilience Plan, Mission 4 Component 2 Investment 3.1 “Fund for the realisation of an integrated system of research and innovation infrastructures”-Call for tender No. 3264 of 28 December 2021 of the Italian Ministry of University and Research funded by the European Union—NextGenerationEU—PNRR IR0000020, Concession Decree No. 244 of 8 August 2022 adopted by the Italian Ministry of University and

Research, CUP F53C22000560006, ECCSELLENT—Development of ECCSEL-R.I. Italian facilities: user access, services and long-term sustainability.

Data Availability Statement: Data are contained within the article.

Acknowledgments: The authors thank Dario Santonocito from the University of Messina, Italy, for the compression tests performed on the investigated samples. Paolo Giorgianni from Signo Motus srl, Messina, Italy, is also acknowledged for the determination of the rheological properties of the prepared catalytic pastes.

Conflicts of Interest: The authors declare no conflicts of interest.

References

1. Solarin, S.A. An environmental impact assessment of fossil fuel subsidies in emerging and developing economies. *Environ. Impact Assess. Rev.* **2020**, *85*, 106443–106451. [[CrossRef](#)]
2. Kalair, A.; Abas, N.; Saleem, M.S.; Kalair, A.R.; Khan, N. Role of energy storage systems in energy transition from fossil fuels to renewables. *Energy Storage* **2020**, *3*, 135–161. [[CrossRef](#)]
3. Semelsberger, T.A.; Borup, R.L.; Greene, H.L. Dimethyl ether (DME) as an alternative fuel. *J. Power Sources* **2006**, *156*, 497–511. [[CrossRef](#)]
4. Azizi, Z.; Rezaeimanesh, M.; Tohidian, T.; Rahimpour, M.R. Dimethyl ether: A review of technologies and production challenges. *Chem. Eng. Process. Process Intensif.* **2014**, *82*, 150–172. [[CrossRef](#)]
5. Parekh, A.; Chaturvedi, G.; Dutta, A. Sustainability analyses of CO₂ sequestration and CO₂ utilization as competing options for mitigating CO₂ emissions. *Sustain. Energy Technol. Assess.* **2023**, *55*, 102942–102948. [[CrossRef](#)]
6. Mota, N.; Ordoñez, E.M.; Pawelec, B.; Fierro, J.L.G.; Navarro, R.M. Direct Synthesis of Dimethyl Ether from CO₂: Recent Advances in Bifunctional/Hybrid Catalytic Systems. *Catalysts* **2021**, *11*, 411–444. [[CrossRef](#)]
7. Bonura, G.; Todaro, S.; Frusteri, L.; Majchrzak-Kuceba, I.; Wawrzyńczak, D.; Pászti, Z.; Tálas, E.; Tompos, A.; Lonyi, F.; Solt, H.; et al. Inside the reaction mechanism of direct CO₂ conversion to DME over zeolite-based hybrid catalysts. *Appl. Catal. B* **2021**, *294*, 120255–120264. [[CrossRef](#)]
8. Bonura, G.; Cannilla, C.; Frusteri, L.; Catizzzone, E.; Todaro, S.; Migliori, M.; Giordano, G.; Frusteri, F. Interaction effects between CuO-ZnO-ZrO₂ methanol phase and zeolite surface affecting stability of hybrid systems during one-step CO₂ hydrogenation to DME. *Catal. Today* **2020**, *345*, 175–182. [[CrossRef](#)]
9. Liu, C.; Liu, Z. Perspective on CO₂ Hydrogenation for Dimethyl Ether Economy. *Catalysts* **2022**, *12*, 1375–1394. [[CrossRef](#)]
10. Bonura, G.; Frusteri, F.; Cannilla, C.; Drago Ferrante, G.; Aloise, A.; Catizzzone, E.; Migliori, M.; Giordano, G. Catalytic features of CuZnZr-zeolite hybrid systems for the direct CO₂-to-DME hydrogenation reaction. *Catal. Today* **2016**, *277*, 48–54. [[CrossRef](#)]
11. Bonura, G.; Cannilla, C.; Frusteri, L.; Mezzapica, A.; Frusteri, F. DME production by CO₂ hydrogenation: Key factors affecting the behaviour of CuZnZr/ferrierite catalysts. *Catal. Today* **2017**, *281*, 337–344. [[CrossRef](#)]
12. Sathish, K.; Kumar, S.S.; Magal, R.T.; Selvaraj, V.; Narasimharaj, V.; Karthikeyan, R.; Sabarinathan, G.; Tiwari, M.; Kassa, A.E. A Comparative Study on Subtractive Manufacturing and Additive Manufacturing. *Adv. Mat. Sci. Eng.* **2022**, *2022*, 6892641–6892648. [[CrossRef](#)]
13. Revelo, C.F.; Colorado, H.A. 3D printing of kaolinite clay ceramics using the Direct Ink Writing (DIW) technique. *Ceram. Int.* **2018**, *44*, 5673–5682. [[CrossRef](#)]
14. Chen, H.; Wang, J.; Peng, S.; Liu, D.; Yan, W.; Shang, X.; Zhang, B.; Yao, Y.; Hui, Y.; Zhou, N. A Generalized Polymer Precursor Ink Design for 3D Printing of Functional Metal Oxides. *Nano-Micro Lett.* **2023**, *15*, 180–195. [[CrossRef](#)] [[PubMed](#)]
15. Zoude, C.; Gremillard, L.; Prud'Homme, E. Combination of Chemical Foaming and Direct Ink Writing for Lightweight Geopolymers. *Open Ceram.* **2023**, *16*, 123211–123224. [[CrossRef](#)]
16. Murphy, R.D.; Delaney, C.; Kolagatla, S.; Florea, L.; Hawker, C.J.; Heise, A. Design of Statistical Copolypeptides as Multipurpose Hydrogel Resins in 3D Printing. *Adv. Funct. Mater.* **2023**, *33*, 2306710–2306718. [[CrossRef](#)]
17. Gharaie, S.; Zolfagharian, A.; Moghadam, A.A.A.; Shukur, N.; Bodaghi, M.; Mosadegh, B.; Kouzani, A. Direct 3D Printing of a Two-Part Silicone Resin to Fabricate Highly Stretchable Structures. *Prog. Addit. Manuf.* **2023**, *8*, 1555–1571. [[CrossRef](#)]
18. Cagirici, M.; Xun, Y.; Zhang, D.; Xu, X.; Ding, J. Direct Ink Writing of Ni Structures for Electrocatalytic Water Splitting Applications. *Mater. Chem. Phys.* **2024**, *311*, 128574–128580. [[CrossRef](#)]
19. Yang, F.; Zhao, S.; Chen, G.; Li, K.; Fei, Z.; Mummery, P.; Yang, Z. High-Strength, Multifunctional and 3D Printable Mullite-Based Porous Ceramics with a Controllable Shell-Pore Structure. *Adv. Powder Mater.* **2024**, *3*, 100153–100164. [[CrossRef](#)]
20. von Szczepanski, J.; Roels, E.; Siqueira, G.; Danner, P.M.; Wolf, J.; Legrand, J.; Brancart, J.; Terryn, S.; van Assche, G.; Vanderborght, B.; et al. Printable Polar Silicone Elastomers for Healable Supercapacitive Strain Sensors. *Adv. Mater. Technol.* **2023**, *8*, 2301310–2301319. [[CrossRef](#)]
21. van Hazendonk, L.S.; Vonk, C.F.; van Grondelle, W.; Vonk, N.H.; Friedrich, H. Towards a Predictive Understanding of Direct Ink Writing of Graphene-Based Inks. *Appl. Mater. Today* **2024**, *36*, 102014–102025. [[CrossRef](#)]
22. Tay, R.Y.; Song, Y.; Yao, D.R.; Gao, W. Direct-Ink-Writing 3D-Printed Bioelectronics. *Mater. Today* **2023**, *71*, 135–151. [[CrossRef](#)] [[PubMed](#)]

23. Li, Y.; Chen, L.; Stehle, Y.; Lin, M.; Wang, C.; Zhang, R.; Huang, M.; Li, Y.; Zou, Q. Extrusion-Based 3D-Printed “Rolled-up” Composite Scaffolds with Hierarchical Pore Structure for Bone Growth and Repair. *J. Mater. Sci. Technol.* **2024**, *171*, 222–234. [[CrossRef](#)]
24. Wang, Y.; Lin, S.; Li, M.; Zhu, C.; Yang, H.; Dong, P.; Lu, M.; Wang, W.; Cao, J.; Liu, Q.; et al. Boosting CO₂ Hydrogenation of Fe-Based Monolithic Catalysts via 3D Printing Technology-Induced Heat/Mass-Transfer Enhancements. *Appl. Catal. B Environ.* **2024**, *340*, 123211. [[CrossRef](#)]
25. Ngo, T.D.; Kashani, A.; Imbalzano, G.; Nguyen, K.T.Q.; Hui, D. Additive manufacturing (3D printing): A review of materials, methods, applications and challenges. *Compos. B Eng.* **2018**, *143*, 172–196. [[CrossRef](#)]
26. Chapiro, M. Current achievements and future outlook for composites in 3D printing. *Reinf. Plast.* **2016**, *60*, 372–375. [[CrossRef](#)]
27. Tubío, C.R.; Azuaje, J.; Escalante, L.; Coelho, A.; Guitián, F.; Sotelo, E.; Gil, A. 3D printing of a heterogeneous copper-based catalyst. *J. Catal.* **2016**, *334*, 110–115. [[CrossRef](#)]
28. Bonura, G.; Todaro, S.; Middelkoop, V.; de Vos, Y.; Abbenhuis, H.C.L.; Gerritsen, G.; Koekkoek, A.J.J.; Cannilla, C.; Frusteri, F. Effectiveness of the 3D-printing procedure in the synthesis of hybrid catalysts for the direct hydrogenation of CO₂ into dimethyl ether. *J. CO₂ Util.* **2023**, *70*, 102458–102463. [[CrossRef](#)]
29. Koltsakidis, S.; Koidi, V.; Lappas, A.; Heracleous, E.; Tzetzis, D. Influence of binder concentration in zeolitic ZSM-5/bentonite 3D-printed monoliths manufactured through robocasting for catalytic applications. *Int. J. Adv. Manuf. Technol.* **2023**, *126*, 259–271. [[CrossRef](#)]
30. Chen, C.H.; Chang, Y.; Wang, C.C.; Huang, C.H.; Huang, C.C.; Yeh, Y.C.; Hwang, S.M.; Sung, H.W. Construction and characterization of fragmented mesenchymal-stem-cell sheets for intramuscular injection. *Biomaterials* **2007**, *28*, 4643–4651. [[CrossRef](#)]
31. Polamaplyya, P.; Chengb, Y.; Shib, X.; Manikandana, K.; Kremera, G.E.; Qin, H. 3D Printing and Characterization of Hydroxypropyl Methylcellulose and Methylcellulose for Biodegradable Support Structures. *Procedia Manuf.* **2019**, *34*, 552–559. [[CrossRef](#)]
32. Finny, A.S.; Cheng, N.; Popoola, O.; Andreescu, S. 3D printable polyethyleneimine based hydrogel adsorbents for heavy metal ions removal. *Environ. Sci. Adv.* **2022**, *1*, 443–456. [[CrossRef](#)]

Disclaimer/Publisher’s Note: The statements, opinions and data contained in all publications are solely those of the individual author(s) and contributor(s) and not of MDPI and/or the editor(s). MDPI and/or the editor(s) disclaim responsibility for any injury to people or property resulting from any ideas, methods, instructions or products referred to in the content.